

Influence of structural anisotropy to anisotropic electron mobility in a-plane InN

H. Ahn, J.-W. Chia, H.-M. Lee, and S. Gwo

Citation: [Applied Physics Letters](#) **102**, 061904 (2013); doi: 10.1063/1.4792209

View online: <http://dx.doi.org/10.1063/1.4792209>

View Table of Contents: <http://scitation.aip.org/content/aip/journal/apl/102/6?ver=pdfcov>

Published by the [AIP Publishing](#)

Articles you may be interested in

[Electron mobility of ultrathin InN on yttria-stabilized zirconia with two-dimensionally grown initial layers](#)

Appl. Phys. Lett. **102**, 022103 (2013); 10.1063/1.4776210

[Temperature dependent effective mass in AlGaIn/GaN high electron mobility transistor structures](#)

Appl. Phys. Lett. **101**, 192102 (2012); 10.1063/1.4765351

[m -plane \(10 1 0 \) InN heteroepitaxied on \(100 \) - LiAlO 2 substrate: Growth orientation control and characterization of structural and optical anisotropy](#)

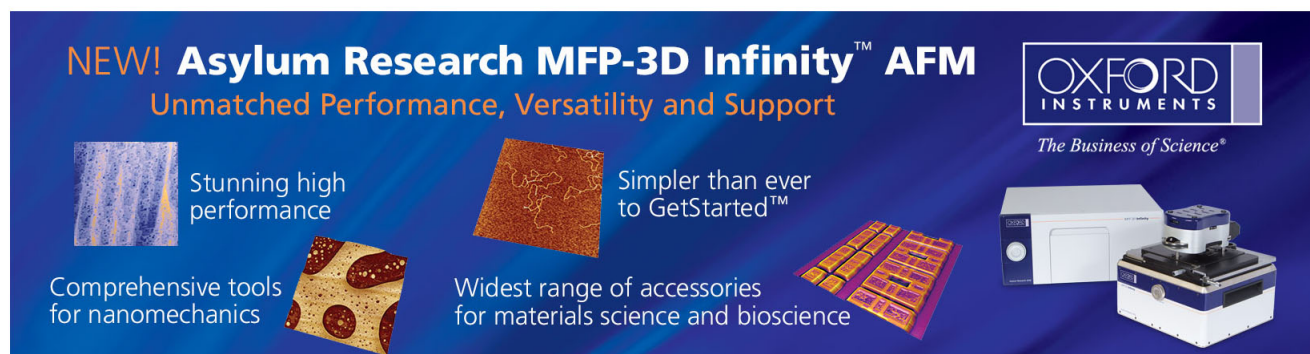
J. Appl. Phys. **107**, 073502 (2010); 10.1063/1.3359680

[Epitaxial growth, electrical and optical properties of a -plane InN on r -plane sapphire](#)

J. Appl. Phys. **107**, 024506 (2010); 10.1063/1.3284086

[High electron mobility InN](#)

Appl. Phys. Lett. **90**, 162103 (2007); 10.1063/1.2722693

The advertisement features a dark blue background with white and orange text. At the top left, it says 'NEW! Asylum Research MFP-3D Infinity™ AFM' in large white letters, followed by 'Unmatched Performance, Versatility and Support' in orange. To the right is the Oxford Instruments logo, which includes the text 'OXFORD INSTRUMENTS' and 'The Business of Science®'. Below the main text are four images with descriptive text: 1) A blue textured surface with the text 'Stunning high performance'. 2) A brown textured surface with the text 'Simpler than ever to GetStarted™'. 3) A yellow and red patterned surface with the text 'Comprehensive tools for nanomechanics'. 4) A white and blue AFM instrument with the text 'Widest range of accessories for materials science and bioscience'. The AFM instrument is shown in a three-quarter view.

Influence of structural anisotropy to anisotropic electron mobility in *a*-plane InN

H. Ahn,^{1,a)} J.-W. Chia,¹ H.-M. Lee,¹ and S. Gwo²

¹Department of Photonics and Institute of Electro-Optical Engineering, National Chiao Tung University, Hsinchu 30010, Taiwan

²Department of Physics, National Tsing Hua University, Hsinchu 30013, Taiwan

(Received 16 October 2012; accepted 31 January 2013; published online 12 February 2013)

This study reports on the anisotropic electron transport properties and a correlation between the electron mobility (μ) and the stacking faults (SFs) in the *a*-plane InN film. Electron mobilities measured by terahertz time-domain spectroscopy and Hall effect measurement along the in-plane $[\bar{1}100]$ (c_{\perp}) orientation were much higher than those of the in-plane $[0001]$ (c_{\parallel}) orientation. This result shows a sharp contrast to higher defect density for the c_{\perp} orientation as measured by x-ray diffraction. The electrons transporting through the planar SFs aligned along the c_{\perp} direction are expected to experience more scattering by defects, resulting in lower μ for the c_{\parallel} orientation.

© 2013 American Institute of Physics. [<http://dx.doi.org/10.1063/1.4792209>]

Since the discovery of its narrow bandgap (~ 0.65 eV), research activities in indium nitride (InN) have been dramatically increased due to its potential applications in high-frequency electronic devices, near-infrared optoelectronics, and high-efficiency solar cells. Its high electron mobility and low interband absorption also make InN be a promising source of terahertz radiation.^{1–4} However, the performance of short-wavelength optoelectronic devices based on $[0001]$ -oriented films can be limited by the polarization-induced internal electric fields. Recently, InN with nonpolar (either *a*- or *m*-axis) surface orientations has attracted considerable attraction due to the possibility to avoid or minimize the built-in electric fields and increase the efficiency of the devices.⁵ However, the *a*-plane InN films contain a higher density of defects consisting of dislocations, stacking faults (SFs), and prismatic stacking faults, in comparison to the *c*-plane films. Therefore, the characteristics of nonpolar InN seriously depends on the growth of high crystalline quality *a*-plane InN films. The reported electron mobility values of nonpolar InN are much smaller than those of the *c*-plane InN films, and the carrier concentrations are generally higher than those of the *c*-plane films.

Typically, nonpolar InN films have been grown on *r*-plane sapphire and the structural properties of the nonpolar InN films are expected to be anisotropic due to the anisotropies of substrate surfaces. This structural anisotropy affects the fundamental film properties such as electron mobility. Several results on these anisotropies have been reported by using ellipsometry, photoluminescence, and x-ray diffraction (XRD) measurements.^{6–9} Meanwhile, despite the previous extensive efforts on the study of structural anisotropy of nonpolar InN, the relation between anisotropy of optical/electrical properties and structural anisotropy has not well been understood. In this work, we investigated the anisotropy of the dispersion relation and the electrical properties of *a*-plane InN in terahertz range by employing terahertz time-domain spectroscopy (THz-TDS). The complex refractive index and electron mobility showed the anisotropy along the *in-plane* $[0001]$ (c_{\parallel})

and $[\bar{1}100]$ (c_{\perp}) orientations and their frequency dependences analyzed with Drude model were discussed in terms of structural anisotropy associated with the carrier scattering time.

An *a*-plane InN epitaxial film (~ 1.2 μm) was grown by plasma-assisted molecular beam epitaxy (PA-MBE) on *r*-plane $\{1\bar{1}02\}$ sapphire wafer. The back side of *r*-plane sapphire wafer was coated with a Ti layer for efficient and uniform heating during the PA-MBE growth and before terahertz transmission measurement, Ti layer was removed by diluted HCl etching. The crystal structure and surface morphology were investigated by high resolution XRD and field-emission scanning electron microscopy (SEM), respectively. The transport properties, such as carrier concentration (N) and the mobility (μ), were studied by Hall effect measurements at room temperature. Especially, in order to measure the dependence of Hall mobility (μ_{Hall}) on the *in-plane* polarization orientation, two narrow strip-shaped samples were prepared by cutting the *a*-plane film along *in-plane* $[\bar{1}100]$ and $[0001]$ orientations, respectively. With the width-to-length ratio of ≤ 5 for each strip-shaped sample, the measured Hall mobilities of c_{\perp} and c_{\parallel} orientations are 359 and 184 cm^2/Vs , respectively, clearly exhibiting the anisotropic transport property.

The THz-TDS system is a contactless method that provides the complex-valued, frequency-dependent electrical conductivity, carrier density, and dispersion responses. In particular, THz-TDS measures both the amplitude and the phase of the terahertz electric field so that the absorption coefficient and refractive index can be extracted without using the Kramers-Kronig analysis. The THz-TDS system is based on *p*-type InAs emitter excited and probed by a Ti:sapphire laser which delivers ~ 150 fs optical pulses at a center wavelength of 800 nm and a repetition rate of 1 kHz. In order to measure the anisotropic response of *a*-plane InN, the sample was rotated about the surface normal and normally transmitted terahertz signal through the sample is detected by free-space electro-optic sampling method.

The SEM image of the *a*-plane InN film in Fig. 1(a) exhibits the characteristic wavy, striped morphology perpendicular to the *in-plane* *c*-direction. The anisotropic *in-plane*

^{a)}Author to whom correspondence should be addressed. Electronic mail: hyahn@mail.nctu.edu.tw.

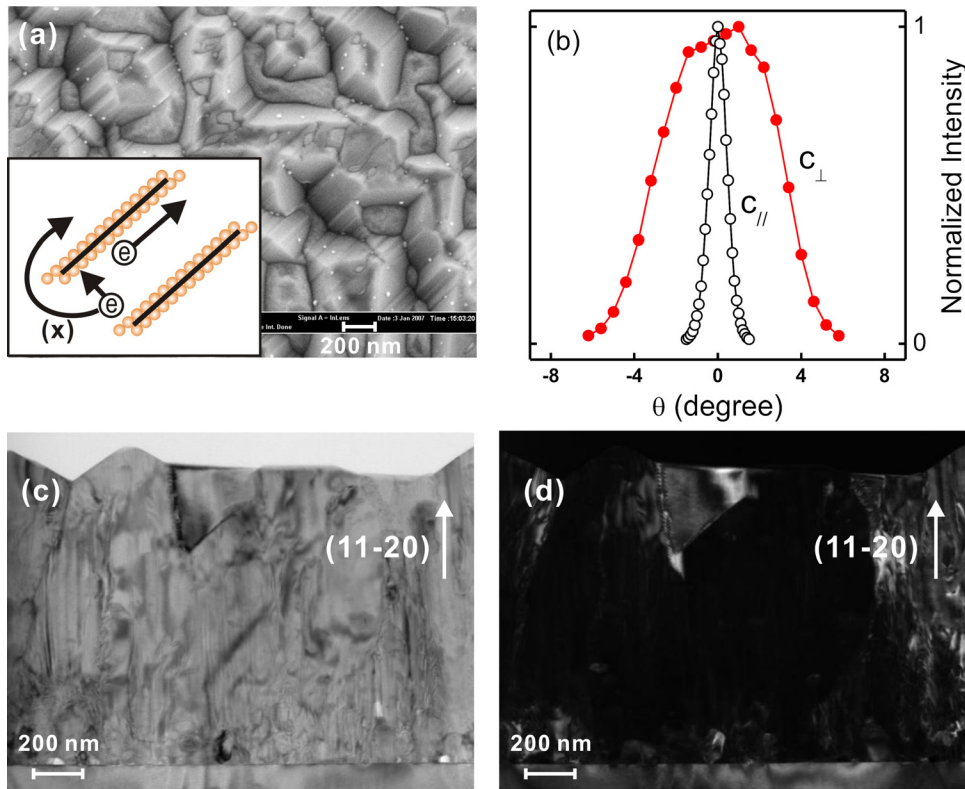


FIG. 1. (a) Top-view SEM image of a nonpolar (*a*-plane) InN film, grown on *r*-plane sapphire substrates by nitrogen-plasma-assisted molecule beam epitaxy. (b) ω - 2θ XRD rocking curves of the *a*-plane InN peak taken with an open detector parallel and perpendicular to the *in-plane* *c*-axis showing significant anisotropy. (c) and (d) Cross-sectional bright-field and dark-field TEM images for the $[\bar{1}100]$ zone axis from an *a*-plane InN film, respectively. Inset: Scheme of electron transport along and through the SFs. Since electrons cannot detour around the long channel of SFs, electrons transporting parallel to the *in-plane* *c*-axis can be quickly scattered or trapped by the defects.

strain and/or adatom diffusion length in nonpolar InN are suggested to modify the growth front and result in the anisotropic surface morphology.^{10,11} The growth direction of the InN film was determined using ω - 2θ XRD scans around the (11 $\bar{2}$ 0) InN reflection. Besides the sapphire (1 $\bar{1}$ 02) and (2 $\bar{2}$ 04) Bragg reflections, the InN (11 $\bar{2}$ 0) peak could be detected without any other extra peaks, such as wurtzite (0002) peak or zinc-blender InN phase. The *in-plane* epitaxial relationship between *a*-plane InN and *r*-plane sapphire is identical to that reported by Lu *et al.*,¹² such that $[0001]_{\text{InN}} \parallel [\bar{1}100]_{\text{Al}_2\text{O}_3}$ and $[\bar{1}100]_{\text{InN}} \parallel [11\bar{2}0]_{\text{Al}_2\text{O}_3}$. Figure 1(b) shows the full widths at half maximum (FWHM) of the rocking curves taken along the two orthogonal *in-plane* [0001] and $[\bar{1}100]$ orientations. The rocking curve FWHM of the c_{\perp} orientation is 6.1° , while that of the c_{\parallel} orientation is $\sim 1^{\circ}$. The broader rocking curve of nonpolar InN may be due to anisotropic distribution of dislocations, tilt, wafer bending, and SFs. Figures 1(c) and 1(d) are the cross-sectional bright-field and dark-field TEM images, respectively. In the bright-field image, many basal-plane SFs are shown as propagating straight lines to the surface. Generally, in the dark-field image, defects that produce only displacement of atoms, such as SFs, cannot be easily seen.¹³ Therefore, in Fig. 1(d), dislocations appear as white lines, whereas most of SFs appear dim. Only within the first ~ 100 nm of InN growth, dislocation network with closed loops is observed, otherwise the density of dislocations is low through the whole film. Considering the small synchrotron-radiation x-ray beam size used for XRD measurement, the contribution of wafer bending to the broadening of XRD curve can be negligible. These results then indicate that the main structural defects in our *a*-plane film are SFs associated with anisotropic strain in nonpolar film, similar to most of heteroepitaxial nonpolar wurtzite films.^{10,14}

Figure 2 exhibits the terahertz transmittance of the *a*-plane InN film measured along the c_{\perp} and c_{\parallel} orientations, in which the transmittance along the c_{\parallel} orientation is at least twice larger than that along c_{\perp} orientation. From this anisotropic terahertz transmittance, the complex refractive index (\tilde{n}) and the electrical conductivity ($\tilde{\sigma}(\omega) = \sigma_1 + i\sigma_2$) are calculated and illustrated in Fig. 3. We fit the measured complex conductivity in Figs. 3(b) and 3(d) using the simple Drude model, in which the complex conductivity is defined by

$$\tilde{\sigma}(\omega) = \varepsilon_0 \omega_p^2 \tau_0 / (1 - i\omega\tau_0), \quad (1)$$

where $\omega_p^2 = Ne^2 / (m^* \varepsilon_0)$ is the plasma frequency and τ_0 is the carrier scattering time. Solid lines are obtained with the fitting parameters $\omega_p / 2\pi = 83 \pm 1.2$ THz for both orientations and $\tau_0 = 18$ and 8 fs for the c_{\perp} and c_{\parallel} orientations, respectively.

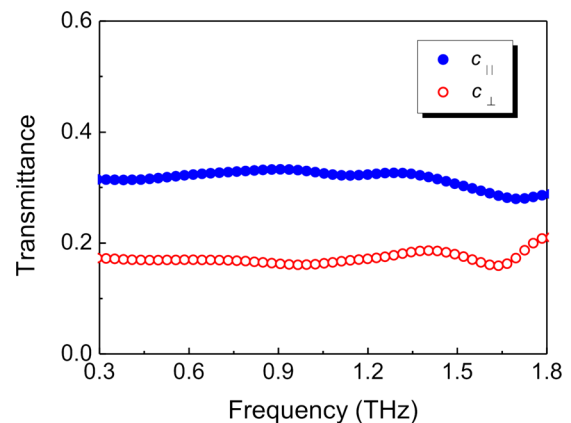


FIG. 2. Terahertz transmittance of a nonpolar InN film measured for the linear polarization states parallel (solid circles) and perpendicular (open circles) to the *in-plane* *c*-axis.

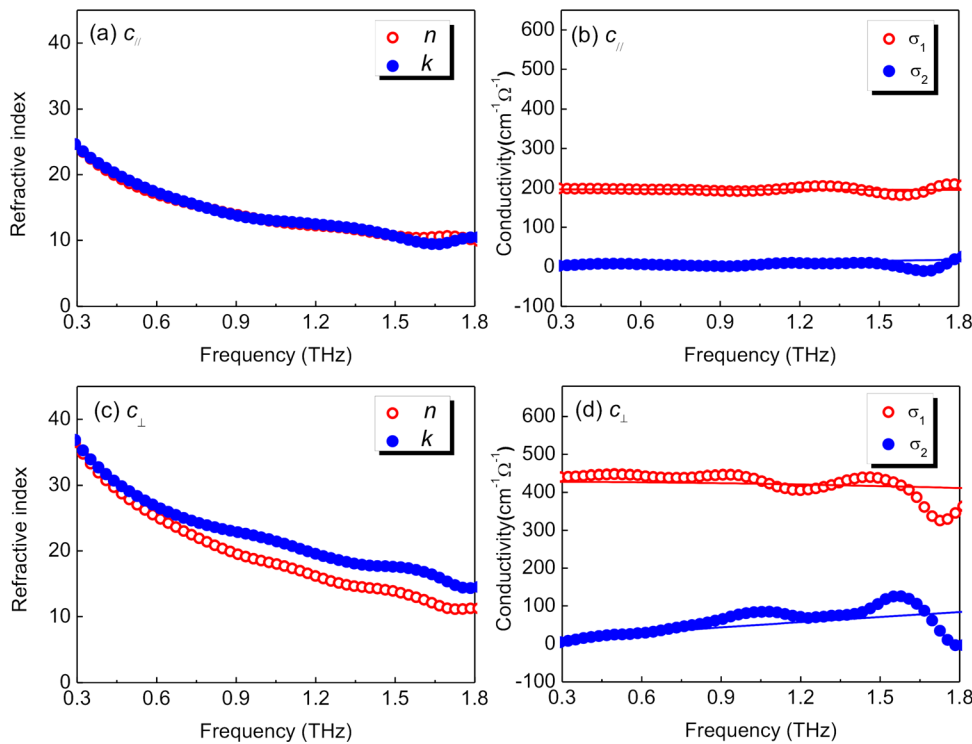


FIG. 3. *In-plane* polarization dependence of the complex refractive index and electrical conductivity of the nonpolar InN film, extracted from the terahertz transmittance curve in Fig. 2. Solid lines in (b) and (d) are obtained by the simple Drude model with the parameters listed in Table I.

From the fitting parameters, an electron density (N_{TDS}) of $0.8 \times 10^{19} \text{ cm}^{-3}$ for both orientations and anisotropic electron mobilities ($\mu_{\text{TDS}} = e\tau_0/m^*$) of 333 and 148 cm^2/Vs were extracted for the c_{\perp} and c_{\parallel} orientation, respectively. It is worthy of noting that these values are in good agreement with those of Hall effect measurement, $N_{\text{Hall}} = 1.1 \times 10^{19} \text{ cm}^{-3}$ and $\mu_{\text{Hall}} = 359$ and 184 cm^2/Vs , respectively.

A large variation in mobility values for nonpolar InN has been reported, and these values are mainly influenced by crystalline quality of the InN films. The Drude model in Eq. (1) treats conduction electrons as free to move and subject to a collisional damping force. And the carrier-carrier scattering time τ_0 obtained in THz-TDS measurement corresponds to the average time between collisions. Therefore, for *a*-plane InN, much shorter carrier scattering time along the c_{\parallel} orientation than that along the c_{\perp} orientation in Table I implies that the carriers in the c_{\parallel} direction experience more collision with defects and quickly damp.

The stacking sequence of InN is *ABAB*... along the wurtzite *c*-axis direction so that the SFs in InN are planar defects and aligned perpendicular to the *in-plane* *c*-axis. The width of the SF is much narrower than its length,¹⁴ and the electrons cannot detour around the long channel of scattering obstacles. Therefore, the orientation of SFs can play an important role in the determination of the electron scattering rate. A broader FWHM of the rocking curve for the c_{\perp}

orientation as shown in Fig. 1(b) indicates that there is a high density of SFs along this orientation. However, for electrons transporting along the c_{\perp} orientation, the extension of SFs is parallel to the motion of electrons so that electrons can travel longer distance before interacting with the SF-associated defects and τ_0 can be longer, as it can be seen in the inset of Fig. 1. In contrast, electrons travelling in the c_{\parallel} direction can experience more scattering with SFs aligned perpendicular to the motion of electrons, resulting in a short carrier scattering time as measured in the THz-TDS experiment. Consequently, the anisotropy in electron mobility may result from the anisotropy of electron scattering by the planar SFs.

In summary, we have performed THz-TDS on MBE-grown *a*-plane InN film and found anisotropic characteristic at terahertz frequency. Nonpolar InN film shows a strong anisotropy of electron mobility, maximum for the in-plane $[\bar{1}100]$ orientation and minimum for the in-plane $[0001]$ orientation. The large anisotropy in electron mobility for *a*-plane InN strongly correlates with the carrier scattering time associated with the structural defects. The microstructure of the nonpolar InN film is dominated by the presence of stacking faults. Since the stacking faults are planar defects, the electron transport through the stacking faults is strongly influenced by the alignment orientation of the stacking faults. Understanding the structure-originated mobility anisotropy can be useful for the growth of high device quality nonpolar InN.

TABLE I. Extracted parameters for best fits in Fig. 3 compared to those obtained from Hall effect measurements.

Polarization	$\omega_p/2$ (THz)	τ_0 (fs)	N_{TDS} ($\times 10^{19}$ cm^{-3})	N_{Hall} ($\times 10^{19}$ cm^{-3})	μ_{TDS} ($\text{cm}^2/\text{V s}$)	μ_{Hall} ($\text{cm}^2/\text{V s}$)
$c_{\text{perpendicular}}$	83	18	0.8	1.1	333	359
c_{parallel}	83	8	0.8	1.1	148	184

This work was supported by the National Science Council (NSC 101-2112-M-009-012-MY3) and the Science Vanguard Research Program (NSC-101-2628-M-007-006) in Taiwan.

¹R. Ascáuzubi, I. Wilke, K. Denniston, H. L. Lu, and W. J. Schaff, *Appl. Phys. Lett.* **84**, 4810 (2004).

²B. Pradarutti, G. Matthäus, C. Brückner, S. Riehemann, G. Notni, S. Nolti, V. Cimalla, V. Lebedev, O. Ambacher, and A. Tünnermann, *Proc. SPIE* **6194**, 619401 (2006).

- ³G. D. Chern, E. D. Readinger, H. Shen, M. Wraback, C. S. Gallinat, G. Koblmuller, and J. S. Speck, *Appl. Phys. Lett.* **89**, 141115 (2006).
- ⁴H. Ahn, Y.-P. Ku, Y.-C. Wang, C.-H. Chuang, S. Gwo, and C.-L. Pan, *Appl. Phys. Lett.* **91**, 132108 (2007).
- ⁵D. Segev and C. G. Van de Walle, *Europhys. Lett.* **76**, 305 (2006).
- ⁶K. Wang, T. Yamaguchi, A. Takeda, T. Kimura, K. Kawashima, T. Araki, and Y. Nanishi, *Phys. Status Solidi A* **207**, 1356 (2010).
- ⁷V. Darakchieva, M.-Y. Xie, N. Franco, F. Giuliani, B. Nunes, E. Alves, C. L. Hsiao, L. C. Chen, T. Yamaguchi, Y. Takagi, K. Kawashima, and Y. Nanishi, *J. Appl. Phys.* **108**, 073529 (2010).
- ⁸P. Schley, J. Rathel, E. Sakalauskas, G. Gobsch, M. Wieneke, J. Blasing, A. Krost, G. Koblmuller, J. S. Speck, and R. Goldhahn, *Phys. Status Solidi A* **207**, 1062 (2010).
- ⁹G. Koblmuller, A. Hirai, F. Wu, C. S. Gallinat, G. D. Metcalfe, H. Shen, M. Wraback, and J. S. Speck, *Appl. Phys. Lett.* **93**, 171902 (2008).
- ¹⁰M. D. Craven, S. H. Lim, F. Wu, J. S. Speck, and S. P. DenBaars, *Appl. Phys. Lett.* **81**, 469 (2002).
- ¹¹H. Wang, C. Chen, Z. Gong, J. Zhang, M. Gaevski, M. Su, J. Yang, and M. Asif Khan, *Appl. Phys. Lett.* **84**, 499 (2004).
- ¹²H. Lu, W. J. Schaff, L. F. Eastman, J. Wu, W. Walukiewicz, V. Cimalla, and O. Ambacher, *Appl. Phys. Lett.* **83**, 1136 (2003).
- ¹³D. Hull and D. J. Bacon, *Introduction to Dislocations* (Oxford, Butterworth-Heinemann, 2001).
- ¹⁴P. Vennéguès, J. M. Chauveau, M. Korytov, C. Deparis, J. Zuniga-Perez, and C. Morhain, *J. Appl. Phys.* **103**, 083525 (2008).